

High field induced magnetic transitions in the $\text{Y}_{0.7}\text{Er}_{0.3}\text{Fe}_2\text{D}_{4.2}$ deuterideV. Paul-Boncour,^{1,*} M. Guillot,² O. Isnard,^{3,4} and A. Hoser⁵¹*Université Paris-Est, Institut de Chimie et des Matériaux Paris-Est (ICMPE; UMR 7182), Centre National de la Recherche Scientifique (CNRS), Université Paris-Est Créteil (UPEC), F-94320 Thiais, France*²*Laboratoire National de Champs Magnétiques Intenses (LNCMI), CNRS, BP166, F-38042 Grenoble Cedex 9, France*³*CNRS, Institut Néel, 25 rue des Martyrs, BP 166X, F-38042 Grenoble, France*⁴*Université Grenoble Alpes, Institut Néel, F-38042 Grenoble, France*⁵*Helmholtz Zentrum Berlin für Materialien und Energie (HZB), Glienicker Str. 100, D-141 09 Berlin, Germany*

(Received 23 May 2017; revised manuscript received 3 July 2017; published 29 September 2017)

The influence of the partial Er for Y substitution on the crystal structure and magnetic properties of $\text{YFe}_2\text{D}_{4.2}$ has been investigated by high field magnetization and neutron diffraction experiments. $\text{Y}_{0.7}\text{Er}_{0.3}\text{Fe}_2\text{D}_{4.2}$ compound crystallizes in the same monoclinic structure as $\text{YFe}_2\text{D}_{4.2}$ described in Pc (P_1c_1) space group with D atoms located in 18 different tetrahedral interstitial sites. A cell volume contraction of 0.6% is observed upon Er substitution, inducing large modification of the magnetic properties. Electronic effect of D insertion as well as lowering of crystal symmetry are important factors determining the magnetic properties of Fe sublattice, which evolves towards more delocalized behavior and modifying the Er-Fe exchange interactions. In the ground state, the Er and Fe moments are arranged ferrimagnetically within the plane perpendicular to the monoclinic b axis and with average moments $m_{\text{Er}} = 6.4(3)\mu_B\text{Er}^{-1}$ and $m_{\text{Fe}} = 2.0(1)\mu_B\text{Fe}^{-1}$ at 10 K. Upon heating, m_{Er} decreases progressively until $T_{\text{Er}} = 55$ K. Between 55 K and 75 K, the Fe sublattice undergoes a first-order ferromagnetic-antiferromagnetic (FM-AFM) transition with a cell volume contraction due to the itinerant metamagnetic behavior of one Fe site. In the AFM structure, m_{Fe} decreases until the Néel temperature $T_{\text{N}} = 125$ K. At high field, two different types of field induced transitions are observed. The Er moments become parallel to the Fe one and saturates to the Er^{3+} free ion value, leading to an unusual field induced FM arrangement at a transition field B_{Trans} of only 78 kG below 30 K. Then above $T_{\text{M0}} = 66$ K, an AFM-FM transition of the Fe sublattice, accompanied by a cell volume increase is observed. B_{Trans} increases linearly versus temperature and with a larger dB_{Trans}/dT slope than for $\text{YFe}_2\text{D}_{4.2}$. This has been explained by the additional contribution of Er induced moments above B_{Trans} .

DOI: [10.1103/PhysRevB.96.104440](https://doi.org/10.1103/PhysRevB.96.104440)**I. INTRODUCTION**

Laves phase AB_2 compounds ($A =$ rare earth; $B =$ 3d transition metal) present a large variety of interesting magnetic properties [1,2]. The AMn_2 intermetallic compounds have been studied for large spin fluctuation and frustrated antiferromagnetic (AFM) Mn sublattices [3–6], AFe_2 compounds for their giant magnetostrictive [1,7,8] and giant magnetoresistance properties [9,10], ACo_2 intermetallic compounds for their itinerant electron metamagnetic (IEM) behavior and magnetocaloric properties [11–15], and ANi_2 for their magnetocaloric properties [16]. In ACo_2 compounds, the IEM behavior of the Co sublattice [17] is still raising interest [14,15]. The application of an external field induces an increase of the density of state (DOS) at the Fermi level $N(E_F)$ that stabilizes the ferromagnetic (FM) state of the Co sublattice. When A is nonmagnetic, the transition field B_{Trans} is large: 700 kG for YCo_2 and 750 kG for LuCo_2 at 4.2 K [12]. The B_{Trans} can be reduced by a modification of the DOS by Al for Co substitution in $\text{A}(\text{Co}_{1-x}\text{Al}_x)_2$ alloys [18,19]. When A is a magnetic rare earth that induces a large molecular field B_m , ACo_2 compounds become FM or ferrimagnetic for light or heavy rare earth, respectively, at 4.2 K [17,20,21].

The AFe_2 compounds are ferrimagnets with Curie temperature ranging from 545 to 785 K, depending on the nature of the rare earth [22]. The Curie temperature can be significantly

reduced by substituting Fe for Al due to a change of the Fe-Fe interactions and interatomic distances by a dilution effect of Fe by Al [23]. A magnetocaloric effect was evidenced in $\text{ErFe}_{2-x}\text{Al}_x$ compounds near their Curie temperature T_C for $x > 1.5$ [23]. The magnetic properties can also be influenced by the nature of the A elements: For example, $(\text{Hf,Ta})\text{Fe}_2$ undergoes a FM-AFM transition attributed to the IEM behavior of one over two Fe sites belonging to the hexagonal $C14$ structure [24–27]. Such IEM behavior is often associated with a significant variation of the magnetic entropy and adiabatic temperature, which can be interesting for applications such as gas liquefaction or magnetic refrigeration [28].

Besides chemical substitution on both A and B sites, hydrogen insertion can be also used to tune significantly the magnetic properties of Laves phase compounds [29,30]. In AFe_2 compounds, hydrogen insertion induces an increase of the cell volume and for some given hydrogen contents a lowering of the crystal symmetry, which changes the magnetic interactions between the atoms. For example, both Curie and compensation temperatures are reduced with increasing H content in ErFe_2 , reflecting a diminution of the Fe-Fe and Er-Fe exchange interactions [31–33]. For large H content, the filling of the DOS by an additional hydrogen electron should also be taken into account. In ErFe_2H_5 , the Fe sublattice remains paramagnetic (PM) down to low temperature, whereas Er moments order in a canted structure below 5 K [34].

The YFe_2H_x hydrides are FM with a decrease of T_C for $x \leq 3.5$, and YFe_2H_5 is PM down to low temperature [35]. The most intriguing properties have been discovered for a

*paulbon@icmpe.cnrs.fr

hydrogen content near $x = 4.2$. The $\text{YFe}_2\text{H}_{4.2}$ displays a first-order FM-AFM transition at $T_{M0} = 131$ K [36–38] and an AFM-PM transition at a Néel temperature $T_N = 165$ K [36,37]. A metamagnetic behavior is observed above T_{M0} with a linear increase of B_{Trans} up to 170 K. This specific magnetic behavior of $\text{YFe}_2\text{D}_{4.2}$ has been explained by a competition between the cell volume increase, which tends to enlarge the mean Fe moment and the formation of strong Fe-H bonds that weaken the Fe-Fe exchange interactions [35]. The concentration $x = 4.2$ H/f.u. is therefore critical, as $\text{YFe}_2\text{H}_{4.2}$ is close to the limit of the FM instability [38]. In addition, the ordering of hydrogen atoms in 18 among 64 tetrahedral interstitial sites induces a lowering of the crystal symmetry from the cubic $C15$ structure toward a monoclinic structure as the temperature decreases below 340 K. In the monoclinic cell (Pc space group), there are eight different Fe sites surrounded by various number of H atoms [39]. The FM-AFM transition has been recently explained by the IEM behavior of one over eight Fe atoms due to both geometric and electronic factors [38]. One of the Fe atoms, which form layers parallel to the (a, c) basal plane and is surrounded by a larger amount of H atoms, loses its moment at the transition, and the coupling between the Fe moments located above and below this plane becomes negative. The AFM structure is formed by FM layers of opposite directions separated by a nonmagnetic layer perpendicular to the monoclinic b axis.

The FM-AFM transition temperature T_{M0} is very sensitive to any cell volume change due to the strong competition between elastic and electronic effects. For example, replacing H by D induces a cell volume reduction of -0.8% and a decrease of T_{M0} from 131 K to 84 K ($\Delta T_{M0} = -47$ K) [37]. The transition temperature decreases also when applying an external pressure: The suppression of the FM ground state is observed for pressures larger than 0.56 GPa for the deuteride and 1.25 GPa for the hydride [40,41]. These results have highlighted the critical role of unit cell volume on the magnetic properties of such $\text{AFe}_2(\text{H,D})_{4.2}$ compounds.

Another way to reduce the cell volume is to substitute Y by another rare earth element of smaller radius like Er. A preliminary work on $\text{Y}_{0.7}\text{Er}_{0.3}\text{Fe}_2(\text{H,D})_{4.2}$ compounds has shown that the Er substitution induces a cell volume reduction and a decrease of T_{M0} for both hydride and deuteride compared to nonsubstituted compounds [42]. Moreover, an additional magnetic transition showing a metamagnetic behavior has been observed below 50 K for these compounds but not for $\text{YFe}_2(\text{H,D})_{4.2}$ compounds. As Er is a magnetic rare earth, the modification of the Er-Fe exchange interaction by H or D insertion should also be taken into account to explain this additional transition.

The first aim of this paper is to observe the influence of the Er substitution on the FM-AFM transition and to compare this chemical pressure effect with that previously studied by applying an external pressure. The second objective is to clarify the physical origin of the new intriguing metamagnetic transition observed at low temperature related to the Er substitution but not observed in the parent intermetallic neither in $\text{YFe}_2\text{D}_{4.2}$ compound: Is it due to an IEM effect, a spin reorientation of the magnetic sublattices, or another field induced transition?

To answer these questions, the structural and magnetic properties of $\text{Y}_{0.7}\text{Er}_{0.3}\text{Fe}_2\text{D}_{4.2}$ have been investigated by magnetic measurements up to high magnetic fields (350 kG) and neutron powder diffraction (NPD) experiments performed versus temperature and applied magnetic field. These results will be compared to those previously obtained for $\text{YFe}_2\text{D}_{4.2}$ and discussed in comparison to other systems.

II. EXPERIMENTAL TECHNIQUES

The preparation of the $\text{Y}_{0.7}\text{Er}_{0.3}\text{Fe}_2$ intermetallic compounds and of the corresponding deuteride is described in Ref. [43]. The D content in the deuteride was estimated by a volumetric method and was found to be 4.15 ± 0.05 D/f.u. The deuteride was quenched into liquid nitrogen and slowly heated under air to room temperature (RT) in order to passivate the surface and to avoid further deuterium desorption.

The crystal structure was checked by powder x-ray diffraction (XRD) at RT on a D8 Bruker diffractometer ($\text{Cu K}\alpha$ radiation). $\text{Y}_{0.7}\text{Er}_{0.3}\text{Fe}_2$ was found to be single phase and crystallizing in the cubic $C15$ structure with $a = 7.334(1)$ Å.

Below 90 kG, the magnetization measurements were performed using a conventional Physical Properties Measurement System (PPMS-9T) from Quantum Design. Additional measurements were performed in Grenoble High Magnetic Field Laboratory (GHMFL, located in Grenoble, France) in high continuous magnetic field up to 350 kG. The experimental procedures of the magnetic studies are detailed in Ref. [42]. Isothermal variations $M_T(B)$ were then obtained. It is noted that after sweeping the field up and down at a given temperature, the absence of remanent magnetization was checked before increasing of temperature.

The NPD patterns of $\text{Y}_{0.7}\text{Er}_{0.3}\text{Fe}_2\text{D}_{4.2}$ have been recorded at 10 and 300 K on the high resolution 3T2 spectrometer at the Laboratoire Léon Brillouin (LLB, Centre d'études atomiques, Saclay, France) with a wavelength of 1.225 Å. Additional NPD measurements were performed with the D1B instrument at the Institut Laue Langevin (ILL, Grenoble, France) with temperature varying from 2 to 300 K. On the D1B instrument, the diffraction patterns have been recorded over an angular range of 80° (2θ) starting at 3° and using a multidetector with a step width of 0.2° between each of the 400 ^3He detection cells. In this configuration, D1B is operating with a wavelength of $\lambda = 2.52$ Å selected by a (002) Bragg reflection of a pyrolytic graphite monochromator, the take-off angle being 44.2° in 2θ . Due to the high flux available on the instrument, temperature evolution of the diffraction pattern has been recorded *in situ* during heating by recording the diffraction patterns every 3 K. The powder sample was introduced in vanadium cylindrical sample container.

The NPD measurements have been also performed between 2 and 170 K in vertical magnetic field up to 100 kG on E6 focusing diffractometer of Helmholtz Zentrum Berlin (HZB, Germany). The powder sample introduced in an aluminum cylindrical sample container was frozen using deuterated alcohol to avoid preferred orientation of grains with the magnetic field. The selected wavelength was 2.454 Å. The angular range was between $3^\circ < 2\theta < 113^\circ$ with a step width of 0.15° .

TABLE I. Cell parameters of $\text{YFe}_2\text{D}_{4.2}$ and $\text{Y}_{0.7}\text{Er}_{0.3}\text{Fe}_2\text{D}_{4.2}$ measured by XRD and described in Pc space group at RT.

	a (Å)	b (Å)	c (Å)	β (°)	V (Å ³)
$\text{YFe}_2\text{D}_{4.2}$	5.508	11.468	9.426	122.39	503.0
$\text{Y}_{0.7}\text{Er}_{0.3}\text{Fe}_2\text{D}_{4.2}$	5.492	11.450	9.411	122.36	500.0
Relative change (%)	-0.27	-0.16	-0.18	-	-0.60

All the XRD and NPD patterns were refined by Rietveld refinement analysis using the FullProf code [44].

III. EXPERIMENTAL RESULTS AND ANALYSIS

A. Crystal structure at RT

The XRD pattern of $\text{Y}_{0.7}\text{Er}_{0.3}\text{Fe}_2\text{D}_{4.2}$ measured at RT was refined in the same monoclinic structure as $\text{YFe}_2\text{D}_{4.2}$, and their cell parameters are compared in Table I. Although the XRD patterns can be refined in a $C2/m$ monoclinic space group, the NPD pattern analysis has shown a lowering of the crystal symmetry in a primitive monoclinic cell and a doubling of the b parameter, which is due to the ordering of D atoms in preferential interstitial sites. This monoclinic structure can be described in the monoclinic Pc space group (N° 7) [39]. Therefore, to compare the results obtained by both XRD and neutron diffraction, we have presented all the diffraction results in the same primitive monoclinic cell. A larger reduction of the a cell parameter (-0.27%) compared to b and c cell parameters (-0.16 and -0.18%) and a cell volume decrease of 0.6% is observed for the Er substituted compound compared to $\text{YFe}_2\text{D}_{4.2}$.

The NPD pattern of $\text{Y}_{0.7}\text{Er}_{0.3}\text{Fe}_2\text{D}_{4.2}$ at RT was refined starting from the same nuclear structure and atomic positions as $\text{YFe}_2\text{D}_{4.2}$ in Pc space group [39]. At first, the positions of the metallic atoms (Y, Er, and Fe) were fixed equal to those refined for Y and Fe in $\text{YFe}_2\text{D}_{4.2}$, whereas the positions and occupancy factors of all D atoms were refined. The Er was statistically substituted on the Y sites, with the nominal ratio 0.3:0.7 obtained by chemical analysis. Further refinement of Y, Er, and Fe positions slightly improved the quality of the fit, but the atomic positions remained within the experimental error bars. These results are reported in Tables II and III, and the refined NPD pattern of $\text{Y}_{0.7}\text{Er}_{0.3}\text{Fe}_2\text{D}_{4.2}$ at RT is presented versus Q [$Q = 4\pi \cdot \sin(\theta)/\lambda$] in Fig. 1(a). The NPD patterns at 10 and 75 K are given for comparison in Figs. 1(b) and 1(c), respectively, and will be analyzed later.

Similar to the reference $\text{YFe}_2\text{D}_{4.2}$, 15 D atoms are located in tetrahedral $A_2\text{Fe}_2$ interstitial sites and three D atoms (D11, D17, and D18) in tetrahedral $A\text{Fe}_3$ sites ($A = \text{Y, Er}$). The total D content 4.0 ± 0.2 D/f.u. is compatible with the D content estimated by the volumetric method (4.15 D/f.u.). This value is slightly smaller than the D content refined for $\text{YFe}_2\text{D}_{4.2}$ [4.3(1) D/f.u.]. This difference probably arises from the smaller cell volume of the Er containing sample.

The lowering of crystal symmetry in the deuteride implies a larger distance distribution compared to the $\text{Y}_{0.7}\text{Er}_{0.3}\text{Fe}_2$ pristine compound: There are four A and eight Fe sites with different environments instead of one A and one Fe site in the parent alloy. The Fe(A)-D and Fe(A)-Fe distances ($d_{\min}-d_{\max}$

TABLE II. Nuclear cell parameters and magnetic moments obtained from the refinement of the NPD patterns of $\text{Y}_{0.7}\text{Er}_{0.3}\text{Fe}_2\text{D}_{4.2}$ at different temperatures corresponding to the ferrimagnetic (Fe and Er sublattices), antiferromagnetic (Fe sublattice), and paramagnetic states, respectively.

Instrument	(3T2)	(D1B)	(3T2)
T (K)	10	75	293
a (Å)	5.4912(1)	5.4756(1)	5.4885(1)
b (Å)	11.4737(3)	11.4253(3)	11.4503(3)
c (Å)	9.4096(2)	9.3757(1)	9.4042 (2)
β (°)	122.246(1)	122.188 (9)	122.33(1)
V (Å ³)	501.42(2)	496.46(11)	499.39(2)
Magnetic order	Ferri	AFM	PM
$m_{\text{Fe}}(\mu_B)$	2.0(1)	1.79(3)	
$m_{\text{Fe}7}(\mu_B)$	2.0(1)	0	
$m_{\text{Er}}(\mu_B)$	6.4(2)		
θ (°)	-16(5)	-	
φ (°)	90	-	
R_{Bragg} (%)	4.5	3.8	3.6
R_{Mag} (%)	3.8	4.7	-

TABLE III. Atomic positions (x, y, z), occupancy factors (N_{occ}), and Debye-Waller factors (B) resulting from the Rietveld analysis of the $\text{Y}_{0.7}\text{Er}_{0.3}\text{Fe}_2\text{D}_{4.2}$ NPD pattern at 293 K (Pc space group).

atom	x	y	z	N_{occ}	B (Å ²)
Y1/ Er1	0.128(5)	0.122(2)	0.866(3)	0.7/0.3	1.14(4)
Y2/ Er2	0.872(5)	0.374(2)	0.631(3)	0.7/0.3	“ “
Y3/ Er3	0.125(5)	0.382(2)	0.371(3)	0.7/0.3	“ “
Y4/ Er4	0.872(5)	0.125(2)	0.142(3)	0.7/0.3	“ “
Fe1	0.506(5)	0.124(2)	0.505(3)	1.000	1.13(3)
Fe2	0.022(5)	0.127(2)	0.512(3)	1.000	“ “
Fe3	0.492(4)	0.251(1)	0.254(2)	1.000	“ “
Fe4	0.493(5)	0.244(1)	0.743(3)	1.000	“ “
Fe5	0.012(5)	0.375(2)	0.001(3)	1.000	“ “
Fe6	0.491(5)	0.506(1)	0.252(3)	1.000	“ “
Fe7	0.495(5)	0.0007(5)	0.742(5)	1.000	“ “
Fe8	0.504(5)	0.378(2)	0.001(3)	1.000	“ “
D1	0.542(7)	0.622(3)	0.858(4)	0.71(5)	1.68(6)
D2	0.465(8)	0.631(3)	0.144(4)	0.75(5)	“ “
D3	0.469(7)	0.128(3)	0.137(4)	0.82(5)	“ “
D4	0.863(6)	0.284(2)	0.824(3)	1.00(4)	“ “
D5	0.136(6)	0.014(2)	0.649(4)	0.86(5)	“ “
D6	0.145(8)	0.269(3)	0.152(4)	0.79(6)	“ “
D7	0.119(6)	0.775(3)	0.150(4)	0.91(6)	“ “
D8	0.850(7)	0.472(2)	0.821(4)	1.00(5)	“ “
D9	0.854(6)	0.978(2)	0.841(4)	1.00(6)	“ “
D10	0.280(6)	0.453(2)	0.820(4)	0.90(5)	“ “
D11	0.651(5)	0.124(2)	0.725(3)	1.00(4)	“ “
D12	0.712(6)	0.717(2)	0.694(4)	0.93(4)	“ “
D13	0.551(5)	0.239(2)	0.939(3)	0.95(4)	“ “
D14	0.160(7)	0.824(2)	0.901(4)	0.88(5)	“ “
D15	0.830(6)	0.569(2)	0.593(3)	1.00(0)	“ “
D16	0.501(6)	0.980(2)	0.431(4)	0.84(4)	“ “
D17	0.291(7)	0.542(3)	0.547(4)	0.84(5)	“ “
D18	0.716(6)	0.209(2)	0.469(3)	0.94(4)	“ “
$N_{\text{D}}/\text{f.u.}$				4.02 (20)	
$R_{\text{Bragg}} : 3.1\% \quad R_p : 7.37\% \quad R_{\text{wp}} : 7.39\% \quad \text{Chi}_2 : 3.16$					

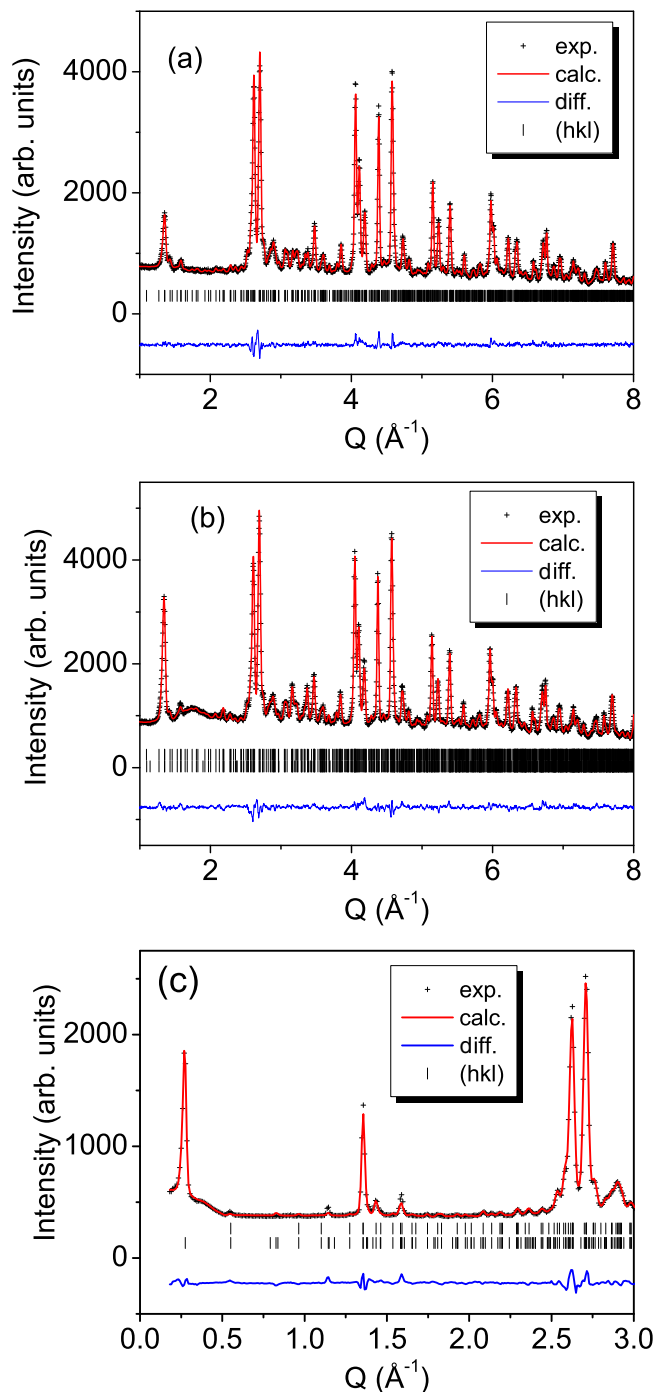


FIG. 1. Refined neutron diffraction patterns of $Y_{0.7}Er_{0.3}Fe_2D_{4.2}$ at 293 K (a), 10 K (b) ($\lambda = 1.225 \text{ \AA}$), and 75 K (c) ($\lambda = 2.52 \text{ \AA}$). The bump in the background around 1.75 \AA^{-1} for the pattern at 10 K is due to the sample holder. (hkl) corresponds to the Bragg peak positions (top = nuclear; bottom = magnetic).

range and average value for each site) are reported in Table IV. The number of D neighbors around each A and Fe site has been calculated using the occupancy factors refined for each D atom. It varies between 7 and 7.8 D at./f.u. for A atoms and 3.7 and 4.6 D at./f.u. for Fe atoms. These later values (Fe-D) are slightly smaller compared to 3.8 – 4.9 D at./f.u. for $YFe_2D_{4.2}$, in agreement with the lower average D content. The Fe-D

distances are ranging between 1.62 and 1.89 \AA , depending on the Fe crystal position, with an average value around $1.72 \pm 0.03 \text{ \AA}$. Each Fe atom is surrounded by six Fe neighbors at $2.81 \pm 0.20 \text{ \AA}$ and six A neighbors at $3.29 \pm 0.20 \text{ \AA}$. Each A atom is surrounded by 12 Fe neighbors at $3.29 \pm 0.17 \text{ \AA}$ and four A neighbors at $3.44 \pm 0.07 \text{ \AA}$. Compared to the parent alloy ($d_{Fe-Fe} = 2.593 \text{ \AA}$, $d_{Fe-A} = 3.040 \text{ \AA}$, and $d_{A-A} = 3.176 \text{ \AA}$), the interatomic distances between metal atoms display an average expansion of 8.3(1)%.

B. Magnetic properties

1. Magnetization measurements

Thermomagnetization curves $M_B(T)$ measured under four different magnetic fields ($B = 0.3, 5, 60,$ and 90 kG) are reported for $Y_{0.7}Er_{0.3}Fe_2D_{4.2}$ in Fig. 2. The $M_B(T)$ curves at 0.3, 5, and 60 kG first increases from low temperature up to a maximum located at $50 \pm 5 \text{ K}$. Then at a temperature T_M , defined as the inflexion point of $dM_B(T)/dT$, a sharp decrease of the $M_B(T)$ curve is observed at $T_M = 59.5 \text{ K}$ for $B = 5 \text{ kG}$ and $T_M = 93.5 \text{ K}$ for $B = 60 \text{ kG}$ (Fig. 2). For an applied field of 90 kG, $M_B(T)$ decreases smoothly from low temperature up to a sharp transition at $T_M = 96.7 \text{ K}$. About 20 K above T_M , a smoother variation of the magnetization is observed for all applied fields.

Isothermal magnetization curves versus field $M_T(B)$ are compared at low temperature range (4.2–53 K) in Fig. 3(a) and at a higher temperature range (80–175 K) in Fig. 3(b). The magnetization of $YFe_2D_{4.2}$ at 4.2 K has been added for comparison in Fig. 3(a). At low temperature and low field ($B \leq 50 \text{ kG}$), the Er contribution significantly reduces the magnetization compared to that of $YFe_2D_{4.2}$. It is also noticeable that for $Y_{0.7}Er_{0.3}Fe_2D_{4.2}$, the saturation of $M_T(B)$ is never reached in the whole 4.2–175 K temperature range even for fields as large as 350 kG, while the saturation was easily reached at high field for $YFe_2D_{4.2}$ [Fig. 3(c)] [37]. This behavior can therefore be attributed to the Er moment contribution. At 175 K, an almost linear increase of $M_T(B)$ versus field takes place.

In both temperature ranges, a field induced metamagnetic behavior is observed but with different characteristics. The transition fields B_{Trans} [maximum of the derivative ($dM/dB)_T$] have been plotted in Fig. 4 versus temperature and compared to those of $YFe_2D_{4.2}$. In this last compound, a metamagnetic behavior was only observed above $T_{M0} = 84 \text{ K}$ and not at low temperature. For $Y_{0.7}Er_{0.3}Fe_2D_{4.2}$, the transition field B_{Trans} is temperature independent and equals $78 \pm 1 \text{ kG}$ for $4.2 < T \leq 30 \text{ K}$. At 36 and 53 K, the metamagnetic transitions are becoming weaker and weaker; however, the transition field B_{Trans} is estimated rapidly increasing with T attaining 120 kG (36 K) and 160 kG (53 K), respectively. Finally, in the 53 to 60 K temperature range, no metamagnetic transitions are observed, with the $M_T(B)$ curves becoming monotonous up to 350 kG. Above T_M , field induced transitions appear again in $Y_{0.7}Er_{0.3}Fe_2D_{4.2}$ [Fig. 3(b)]. The linear extrapolation of B_{Trans} leads to an intercept at zero field $T_{M0} = 66 \text{ K}$, significantly lower than for the nonsubstituted compound ($T_{M0} = 84 \text{ K}$). The influence of the Er content on B_{Trans} is underlined by the inset of Fig. 4, where linear variations of B_{Trans} versus T/T_{M0}

TABLE IV. Number of D atoms around each M atom, M -D, and M -Fe distances (range and average value) of $Y_{0.7}Er_{0.3}Fe_2D_{4.2}$ at 293 K. SD = standard deviation. $A = Y, Er$ and $M = Y, Er, Fe$.

M atom	$N_{occ}(D)$	$d_{min(M-D)} - d_{max(M-D)}$ (Å)	Average d_{M-D} (SD) (Å)	$d_{min(M-Fe)} - d_{max(M-Fe)}$ (Å)	Average d_{M-Fe} (SD) (Å)
A1	7.31(5)	2.14–2.44	2.27(4)	3.06–3.43	3.33(3)
A2	7.20(5)	2.11–2.30	2.21(4)	3.16–3.38	3.28(4)
A3	7.79(5)	2.13–2.48	2.30(4)	3.12–3.45	3.29(4)
A4	7.03(5)	2.13–2.28	2.20(4)	3.05–3.48	3.30(3)
Fe1	3.66(5)	1.68–1.78	1.74(8)	2.66–2.83	2.73(9)
Fe2	4.58(5)	1.58–1.82	1.71(5)	2.68–3.02	2.82(11)
Fe3	4.17(5)	1.62–1.75	1.69(4)	2.74–2.97	2.87(18)
Fe4	4.60(5)	1.67–1.81	1.72(5)	2.66–2.90	2.79(10)
Fe5	4.63(5)	1.66–1.80	1.72(7)	2.67–2.92	2.83(11)
Fe6	4.20(5)	1.66–1.73	1.71(3)	2.66–2.92	2.83(10)
Fe7	4.51(5)	1.68–1.78	1.72(6)	2.66–3.02	2.82(11)
Fe8	4.61(5)	1.63–1.89	1.74(6)	2.66–2.84	2.77(6)

are reported, with the slope in $Y_{0.7}Er_{0.3}Fe_2D_{4.2}$ (2.48 kG/K) being larger than in $YFe_2D_{4.2}$ (1.37 kG/K).

The Arrott-Belov plot at selected temperatures (see the Supplemental Material, Fig. S1 [45]) clearly shows the S shape of the $[M_T(B)]^2$ curves versus B/M above T_M , confirming the first-order character of this IEM transition. The magnetic entropy variation (ΔS_M) reaches 10 J/Kg K^{-1} near T_{M0} for a 0–50 kG field change close to the value obtained for $YFe_2D_{4.2}$ [46]. It is worth mentioning that this corresponds to a large magnitude for a magnetocaloric effect and is comparable to that reported for elemental Gd [47].

Between 4.2 K and T_{M0} , the low field part ($20 \text{ kG} \leq B \leq 60 \text{ kG}$) of each $M_T(B)$ curve is well described (fit accuracy better than 0.5%) by the linear variation [$\chi(T)$ representing the magnetic susceptibility]:

$$M_T(B) = M_{\text{Spont}}(T) + \chi(T) \cdot B \quad (1)$$

except when T is approaching T_{M0} . The extrapolation to zero applied field leads to the spontaneous magnetization (M_{Spont}) whose variation versus temperature is shown in Fig. 5(a). A ferrimagnetic arrangement of the Fe and Er magnetic sublattices is assumed below T_{M0} . Assuming that the mean

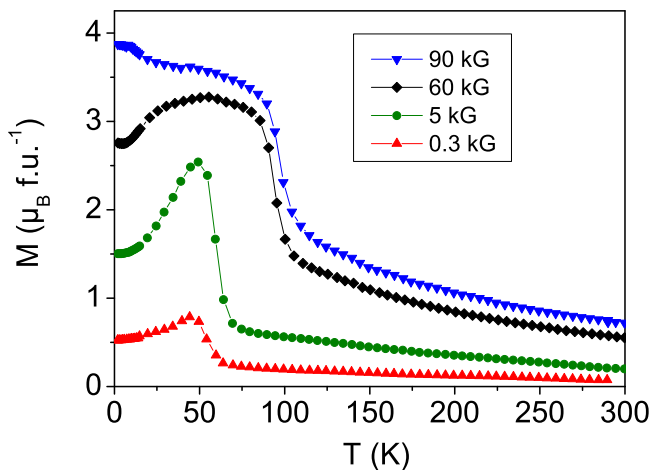


FIG. 2. Thermomagnetization curves of $Y_{0.7}Er_{0.3}Fe_2D_{4.2}$ recorded at different applied fields.

Fe magnetic moment amplitude is not affected by the Er substitution and is given by the spontaneous magnetization measured for $YFe_2D_{4.2}$ ($3.73 \mu_B \text{ f.u.}^{-1}$), the Er moment is found equal to $6.7(2) \mu_B \text{ Er atom}^{-1}$. This value is much smaller than the free atom value ($9 \mu_B \text{ atom}^{-1}$). This difference can be explained by a crystal field effect on the Er atoms, which creates a reduction of the orbital moment of the rare earth. When $T > T_{M0}$ mainly because of the AFM arrangement of the Fe magnetic moments, M_{Spont} becomes smaller and does not exceed $0.35 \mu_B \text{ f.u.}^{-1}$ for both deuterides [Fig. 5(a)].

The saturation magnetizations M_{Sat} were deduced from the extrapolation of the $M_T(B)$ using the $1/B^2$ FM approach law above 150 kG according to

$$M_T(B) = M_{\text{Sat}}(T) \{1 - b_M/B^2\}, \quad (2)$$

where the M_{Sat} determination is being estimated to be of $\pm 3\%$. At 4.2 K, the M_{Sat} and b_M values are found equal to 6.6 (2) $\mu_B \text{ f.u.}^{-1}$ and 5293 kG^2 , respectively. According to the assumptions used for the analysis of the spontaneous magnetization, M_{Sat} is under infinite field the sum of the Fe moment deduced from M_{Sat} in $YFe_2D_{4.2}$ ($m_{\text{Fe}} = 3.8 \mu_B \text{ f.u.}^{-1}$) and of the contribution ($0.3 \times m_{\text{Er}}$) of the Er moment, which is now parallel to the Fe one. At 4.2 K, the calculated moment per Er atom derived from experimental data is then equal to the $9.3 \mu_B \text{ Er atom}^{-1}$, i.e., close to the free atom value. M_{Sat} decreases smoothly when the temperature increases [Fig. 5(b)].

Between T_{M0} and 175 K, each isothermal $M_T(B)$ variation may be divided into three mean parts. At first for $10 \text{ kG} < B < B_{\text{Linear}}$, M remains proportional to B according to Eq. 1; then the metamagnetic transition takes place and is centered on B_{Trans} , which is associated to an abrupt dM_T/dB peak. In the last part, the experimental data are well described by a FM approach law (Eq. (2)). Although the saturation is not reached at 350 kG, the $M_T(B)$ curves diverge from the linearity expected for a PM contribution. An example (at 100 K) of the three field ranges is given in Fig. 3(c), where the crossing field, B_{Crossing} , corresponds to the field at which the magnetizations of the two $Y_{0.7}Er_{0.3}Fe_2D_{4.2}$ and $YFe_2D_{4.2}$ compounds are equal. It is remarked that B_{Crossing} and B_{Trans} are very close.

B_{Linear} (field that marks the upper limit of the linear behavior) varies from 30 kG (121 K) to 200 kG (175 K); the magnetic susceptibility is proportional to the reciprocal

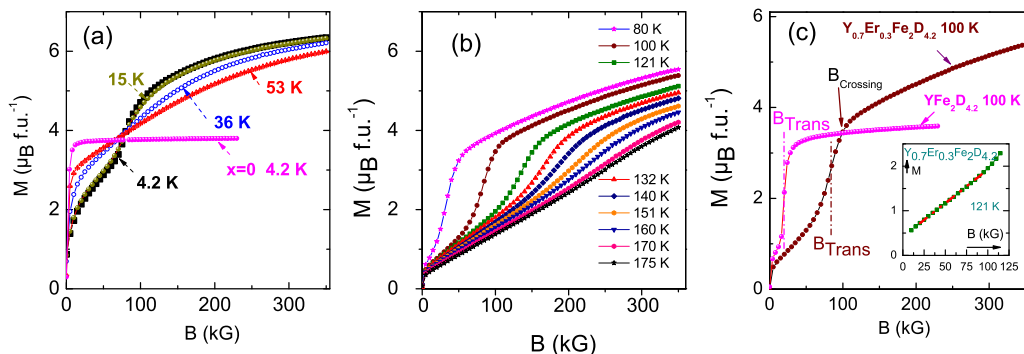


FIG. 3. Magnetization curves of $Y_{0.7}Er_{0.3}FeD_{4.2}$ under high magnetic field (350 kG) between 4.2 and 53 K (a), between 80 and 175 K (b), and at 100 K (c). The $M_T(B)$ curves of $YFe_2D_{4.2}$ have been added at 4.2 K (a) and 100 K (c) for comparison. $B_{Crossing}$ and B_{Trans} in (c) are defined in the text. Inset of (c): linear variation of M versus B at 121 K (i.e., very close to T_N) up to 100 kG.

temperature [Fig. 5(c)] with a pseudo-Curie constant named C_{Exp} and equal to (1.84 ± 0.09) (χ and T being expressed in $\mu_B \text{ mol}^{-1} \text{ kG}^{-1}$ and K, respectively). It is worth noting that the so-determined C_{Exp} value is not very far from the Curie constant ($C = 1$) calculated for two Fe atoms (saturation of $2 \mu_B \text{ atom}^{-1}$).

It is also worth noting that in the 151–175 K range, the variations of $\chi(T)$ for $Y_{0.7}Er_{0.3}Fe_2D_{4.2}$ and $YFe_2D_{4.2}$ compounds are identical [Fig. 5(c)]. In this temperature range, a Curie-Weiss temperature of about 0 K is derived from the linear part of the reciprocal susceptibility versus temperature, indicating a balance between the competing AFM and FM interactions. This result is in agreement with the successive observations of the ferrimagnetic and AFM domains in the magnetic phase diagram of $Y_{0.7}Er_{0.3}Fe_2D_{4.2}$. The large reduction of the magnetic ordering temperature of AF e_2 compounds upon insertion of H or D atoms (about 130 K only for $Y_{0.7}Er_{0.3}Fe_2D_{4.2}$) can be analyzed in the light of the Rhodes and Wohlfarth [48,49] plots as resulting from

an evolution towards a more delocalized character. Taking into account the large unit cell expansion occurring upon H/D insertion in the lattice, one could expect an evolution towards a more localized Fe behavior. However, the observed evolution is opposite, indicating that the effect of hydrogen insertion cannot be restricted to a volume effect and that the electronic effect as well as the lowering of the crystal symmetry are playing an important role in the magnetic properties of the Fe magnetic sublattice in AF $e_2D_{4.2}$ compounds.

In short, the metamagnetic transition observed in the $M_T(B)$ curves at low temperature can be explained by a change of the relative orientation of the Er and Fe moments: antiparallel at low field and parallel at high field, whereas the metamagnetic transition observed above T_{M0} is expected to have a different physical origin, i.e., to be related to the IEM behavior of the Fe sublattice, as observed in $YFe_2D_{4.2}$.

To confirm these assumptions and to get a deeper understanding of the evolution of the magnetic structure of $Y_{0.7}Er_{0.3}Fe_2D_{4.2}$, neutron diffraction experiments have been performed versus temperature and applied field.

2. Neutron diffraction experiments

(a) *Magnetic structures without applied field.* The thermal evolution of the NPD patterns measured on the D1B spectrometer and presented as a three-dimensional (3D) plot in Fig. 6 shows the existence of three different magnetic ranges as the temperature increases from 2 to 300 K. Three characteristic NPD patterns measured at 2, 75, and 200 K are compared in Fig. 7 to observe more clearly the different magnetic peaks.

The magnetic peaks observed in these three ranges are detailed below.

(i) From 2 to 50 K: The NPD pattern at 2 K displays mainly four magnetic peaks at $Q = 1.353 \text{ \AA}^{-1}$ ($d = 4.65 \text{ \AA}$), 1.579 \AA^{-1} ($d = 3.98 \text{ \AA}$), 2.192 \AA^{-1} ($d = 2.88 \text{ \AA}$), and 2.285 \AA^{-1} ($d = 2.75 \text{ \AA}$). The corresponding indexations in the monoclinic nuclear cell are given in Fig. 7. The largest peak ($Q = 1.353 \text{ \AA}^{-1}$) is referred to as NF (0 2 1) and contains both nuclear (37%) and magnetic contribution (63%). The three other peak intensities are weak. The two peaks at 2.192 \AA^{-1} and 2.285 \AA^{-1} are not visible above 50 K and were not observed in the NPD pattern of $YFe_2D_{4.2}$ at low temperature. They can therefore be attributed to the Er magnetic moment contribution and will be noted as Er1 and Er2.

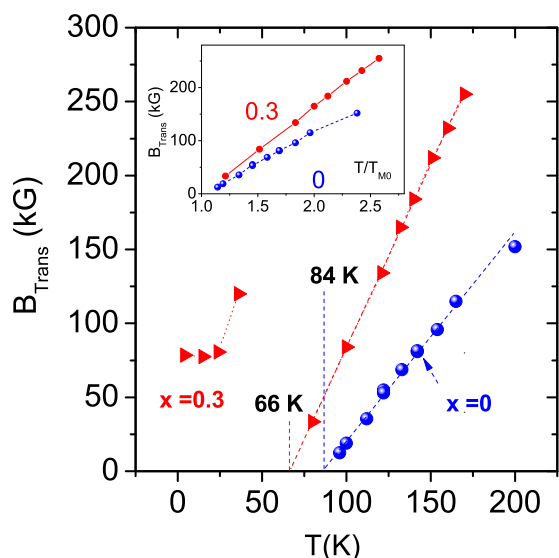


FIG. 4. Transition field B_{Trans} versus temperature for $Y_{1-x}Er_xFe_2D_{4.2}$ deuterides ($x = 0$ and 0.3). T_{M0} is the transition temperature extrapolated at $B = 0$. Inset: B_{Trans} versus the reduced T/T_{M0} variable.

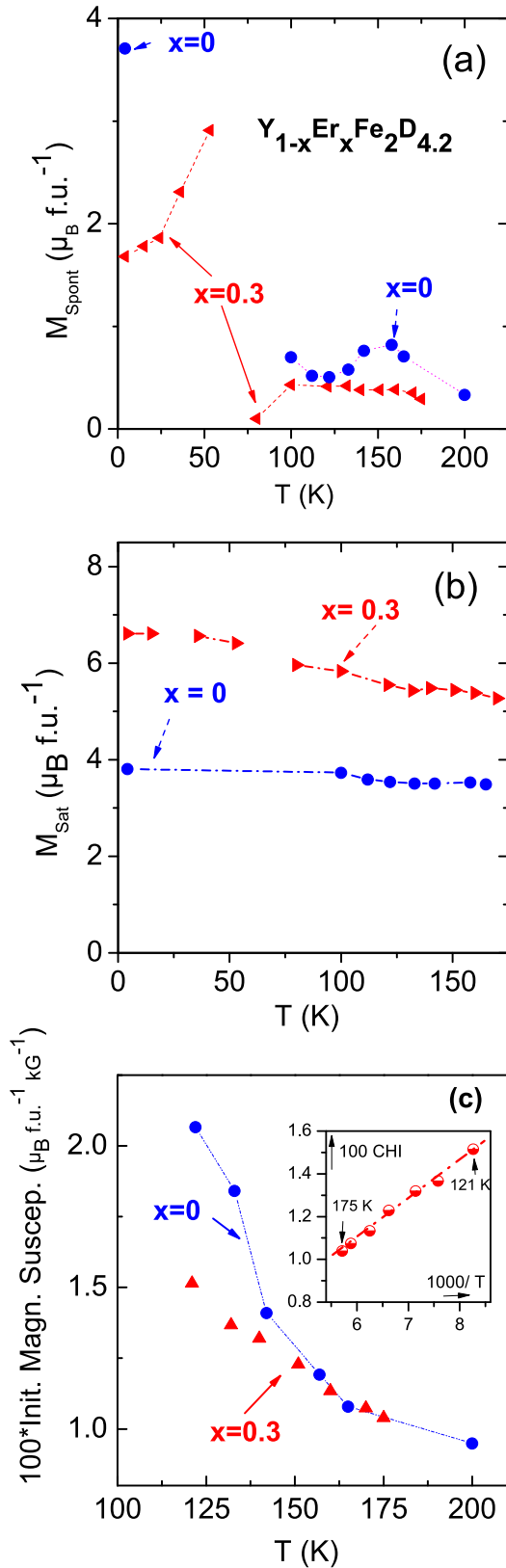


FIG. 5. Spontaneous magnetization (a) and saturation magnetization (b) versus temperature of $YFe_2D_{4.2}$ and $Y_{0.7}Er_{0.3}Fe_2D_{4.2}$. Variation of the initial magnetic susceptibility versus the temperature for the of $YFe_2D_{4.2}$ and $Y_{0.7}Er_{0.3}Fe_2D_{4.2}$ compounds (c). Inset of (c): variation of the $Y_{0.7}Er_{0.3}Fe_2D_{4.2}$ susceptibility versus the reciprocal temperature above the Néel temperature.

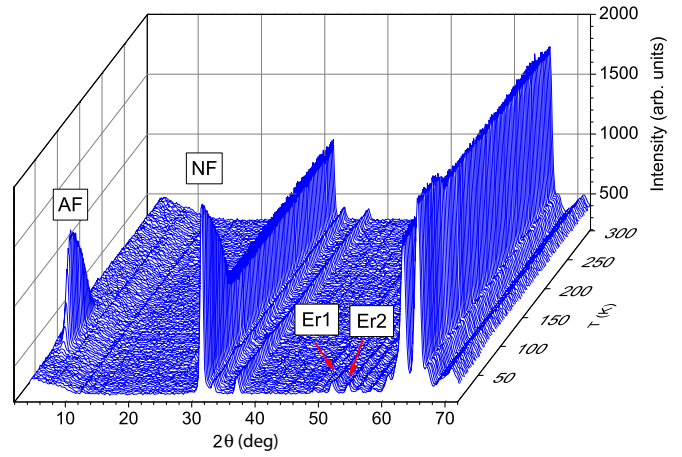


FIG. 6. The 3D representation of the NPD patterns of $Y_{0.7}Er_{0.3}Fe_2D_{4.2}$ measured on D1B diffractometer versus temperature ($\lambda = 2.52 \text{ \AA}$). The figure is plotted between 2 and 72° in order to show the main line intensities.

(ii) From 55 to 125 K: As shown in Fig. 7, the NPD pattern at 75 K displays two additional magnetic peaks at $Q = 0.275 \text{ \AA}^{-1}$ ($d = 22.93 \text{ \AA}$) and 1.144 \AA^{-1} ($d = 5.50 \text{ \AA}$), which are indexed by doubling the cell along the b axis, i.e., in the AFM structure with a $(0, 1/2, 0)$ propagation vector. As similar peaks were previously observed for $YFe_2D_{4.2}$ between 84 and 131 K, the same type of AFM structure is expected for $Y_{0.7}Er_{0.3}Fe_2D_{4.2}$. The peak at 0.275 \AA^{-1} will be noted as AF.

(iii) From 130 to 300 K in this temperature range, the NPD patterns can be refined with only the nuclear structure, as expected from a PM state.

The intensities of the three characteristic magnetic peaks (NF, Er1, and AF) as well as the refined cell volume in all temperature ranges have been plotted versus temperature in Fig. 8. It confirms that the NF peak contains both nuclear and FM intensities, whereas the AF and the Er1 peaks are of purely magnetic origin. Between 2 and 55 K, both NF and

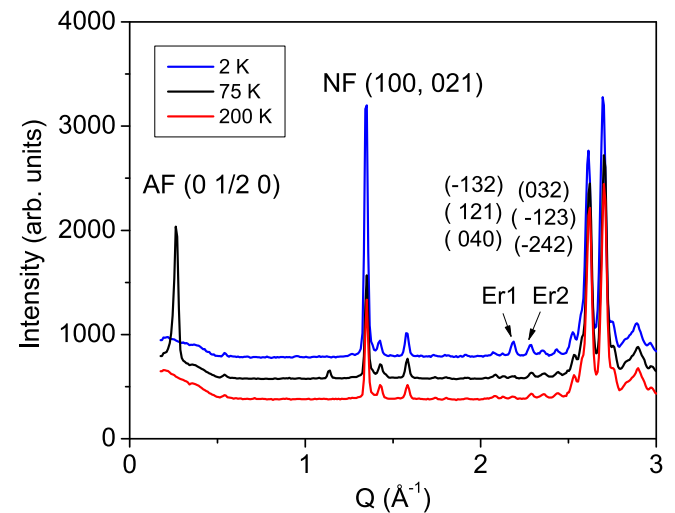


FIG. 7. Comparison of the NPD patterns of $Y_{0.7}Er_{0.3}Fe_2D_{4.2}$ at 2, 75, and 200 K corresponding to ferrimagnetic, antiferromagnetic, and paramagnetic states, respectively ($\lambda = 2.52 \text{ \AA}$).

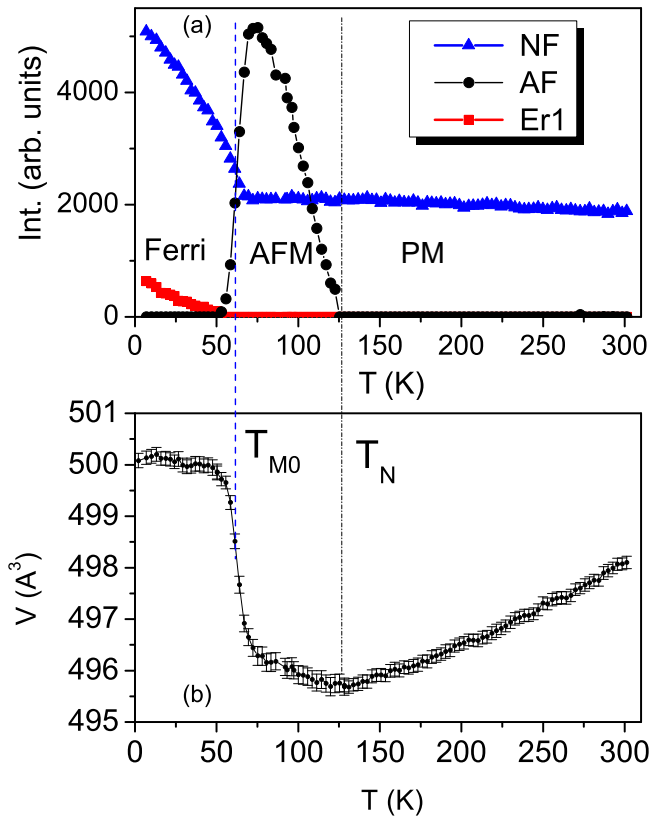


FIG. 8. Evolution of the magnetic peak intensities (a) and cell volume (b) versus temperature of $Y_{0.7}Er_{0.3}Fe_2D_{4.2}$ measured for three Bragg reflections denoted as AF, NF, and Er1 in Fig. 7 (see text). The peak intensity variations allow us to determine the limits of the three magnetic ranges: Ferri, AFM, and PM states.

Er1 peak intensities decrease continuously versus temperature, whereas the unit cell volume decreases slightly. This behavior is attributed to the ferrimagnetic structure, which is abbreviated “Ferri.” Between 55 and 75 K, the intensity of the AF peak increases sharply at the expense of the NF peak, and a cell volume contraction of 0.76% is observed. This corresponds to the sharp decrease of the magnetization observed at T_{M0} . The cell parameter variation reported in the Supplemental Material, Fig. S2 [45], shows a contraction of a , b , and c parameters near T_{M0} upon heating. The contraction is larger for c (−0.37%) and a (−0.25%) than for b (−0.2%). From 75 to 125 K, a continuous decrease of the AF peak intensity is observed, accompanied by a small cell volume decrease of 0.12%. The AFM structure is therefore present between 55 K and $T_N = 125$ K, with a maximum at 75 K. Above T_N , only the nuclear contribution of the NF peak remains, and the cell volume increases again, as expected from the thermal expansion.

The NPD patterns recorded at 10 K (3T2) and 75 K (D1B) were refined in ferrimagnetic and AFM structures, respectively. The magnetic space groups are given in the Supplemental Material (Table S1) [45]. The attempt to refine independently different Fe and Er moments for each Fe and Er site, respectively, leads to nonrealistic values, as it would require a large number of magnetic peaks to refine at least 12 different moments in the ferrimagnetic structure and eight different moments in the AFM structure. As the NPD patterns

contain only four ferrimagnetic peaks and two AFM peaks, respectively, only average values of Fe and Er moments could be obtained from the pattern refinement.

The magnetic structure of $Y_{0.7}Er_{0.3}Fe_2D_{4.2}$ at 10 K was refined using the same spherical description as for $YFe_2D_{4.2}$ [38]: The θ angle and the φ angle are defined as the angles between the Er and Fe moments and the c and b axes, respectively. The NPD pattern was well refined in a collinear ferrimagnetic structure with antiparallel orientation of the Er and Fe moments, as expected for a coupling between heavy rare earth and Fe and in agreement with the magnetization measurements. The result of the refinement is given in Table II, and the refined pattern is presented in Fig. 1(b). The magnitudes of the Er and Fe moments are $\langle m_{Er} \rangle = 6.4(3)$ and $\langle m_{Fe} \rangle = 2.0(1)\mu_B$, respectively, close to the values estimated from the spontaneous magnetizations at 4.2 K ($m_{Er} = 6.7\mu_B$ and $m_{Fe} = 1.87\mu_B$). The θ angle between the Fe moment and the c axis is -16° for a fixed φ angle of 90° . When refined, φ remains close to 90° within the experimental error bar, a confirmation that the magnetic moments remain parallel to the basal plane, with a main contribution along the c axis, as observed also for $YFe_2D_{4.2}$ [38]. The refined value of the Fe moment at 10 K [$m_{Fe} = 2.0(1)\mu_B$] is slightly larger than that refined for $YFe_2D_{4.2}$ [$m_{Fe} = 1.82(3)\mu_B$]. The value of the Er moment [$m_{Er} = 6.4(3)\mu_B$] is close to that refined for $ErFe_2D_5$ at 1.5 K ($m_{Er} = 6.6\mu_B$) [34]. In both systems, the reduction of m_{Er} compared to the Er free ion value ($9\mu_B$) can probably be attributed to a crystal field effect on the Er magnetic moments, as it will be detailed in the discussion.

The evolution of the mean Er and Fe magnetic moments versus temperature was then obtained from the sequential refinement of the NPD patterns measured on D1B (Fig. 9). It confirms the progressive decrease of the Er moment between 2 K and 55 K, whereas the mean Fe moment decreases only slightly until T_{M0} .

The NPD pattern of $Y_{0.7}Er_{0.3}Fe_2D_{4.2}$ at 75 K was refined with the same AFM structure as for $YFe_2D_{4.2}$ with a doubling of the b parameter and considering only an Fe magnetic sublattice, as no Er moment contribution is observed above 55 K [38]. This structure, described in the P_{bc} (No. 7.29) magnetic space group, is constituted of two FM layers with Fe moments perpendicular to the b axis and coupled antiferromagnetically to each other. The inversion of the direction of the Fe moments having components in the basal plane (m_x and m_z) is in agreement with the symmetry operators of the magnetic space group (Supplemental Material, Table S1 [45]). These two FM layers are separated by a nonmagnetic Fe layer, assuming that one among eight Fe atoms loses its moment at the transition through an IEM behavior. According to their atomic positions, only the Fe6 or the Fe7 atoms lies in the same (a , c) plane and can fulfill the geometric condition to form a nonmagnetic Fe layer perpendicular to the monoclinic b axis. As the Fe7 atom has more D neighbors than the Fe6 atom (Table IV), the Fe-D bonds are stronger and favor the transition from a magnetic towards a nonmagnetic state, as detailed in Ref. [38]. The NPD pattern at 75 K was well refined with this AFM structure, and the results of the refinement are summarized in Table II and are shown in Fig. 1(c). At 75 K, the mean Fe moment is $1.79(3)\mu_B$, a value close to that obtained for $YFe_2D_{4.2}$ at 95 K and $YFe_2H_{4.2}$ at 135 K. Although the Mössbauer spectra for

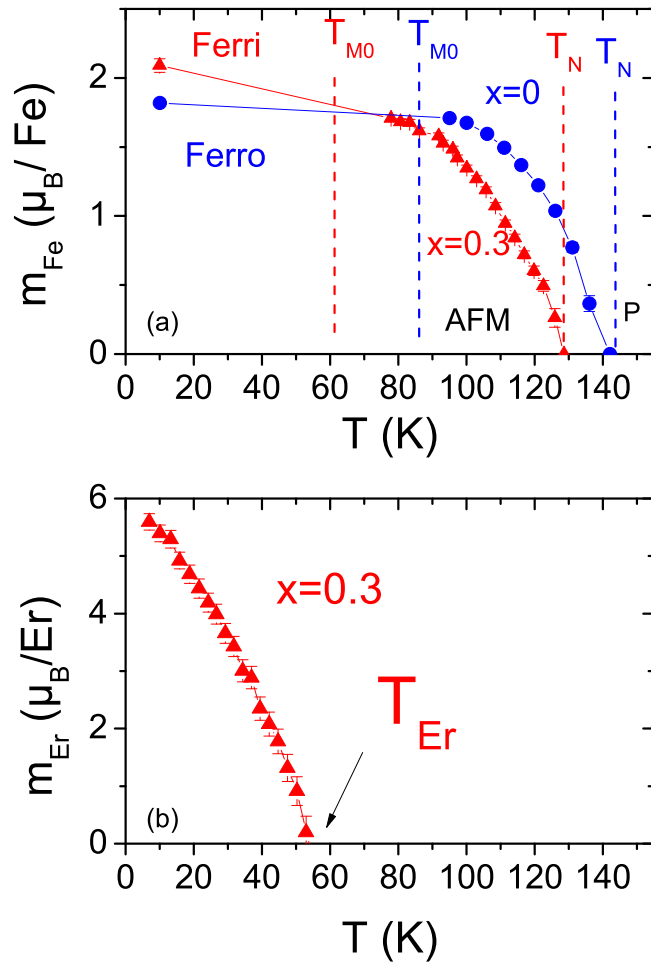


FIG. 9. Comparison of the evolution of the Fe (a) and Er atomic moments (b) versus temperature for $Y_{1-x}Er_xFe_2D_{4.2}$ compounds. The data for $x = 0$ are in blue, and the data for $x = 0.3$ in red (color online).

$Y_{0.7}Er_{0.3}Fe_2D_{4.2}$ have not been measured, it can be assumed that there is also a distribution of Fe moment magnitude due to different number of D neighbors and various Fe-Fe distances, as previously observed for the $YFe_2D_{4.2}$ compound. But due to the limited number of AFM magnetic peaks [50], it was not possible to refine the seven Fe moments independently.

All the NPD patterns measured on D1B between 75 and 125 K were refined with this AFM structure. Figure 9 shows the evolution of the mean Fe moment $\langle m_{Fe} \rangle$ for $Y_{0.7}Er_{0.3}Fe_2D_{4.2}$ compared to that of $YFe_2D_{4.2}$. The same decrease of $\langle m_{Fe} \rangle$ is observed with a shift of 15 K to lower temperature. Similar to $YFe_2(H,D)_{4.2}$ compounds, this variation corresponds to a decrease of the mean Fe moment in each two-dimensional (2D) FM layer.

(b) *Magnetic structures versus field.* The evolution of the NPD patterns under selected applied fields at 2 K is displayed in Fig. 10. The main effect is a decrease of the NF peak intensity versus field [inset of Fig. 10(a)] with a change of slope above 60 kG and an inflexion point at 80 kG. The change of slope corresponds to B_{Linear} , whereas 80 kG corresponds to B_{Trans} at 2 K [Fig. 2(a)]. No variation of the peak position is observed versus temperature, indicating that

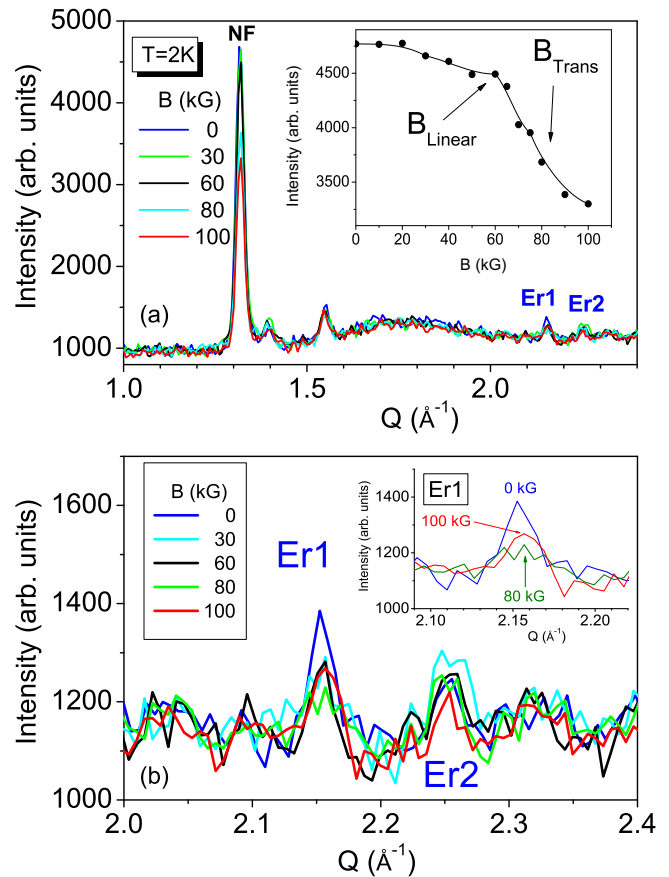


FIG. 10. (a) The NPD patterns of $Y_{0.7}Er_{0.3}Fe_2D_{4.2}$ recorded at 2 K under applied fields of 0, 30, 60, 80, and 100 kG on the E6 spectrometer ($\lambda = 2.454 \text{ \AA}$). Inset: Evolution of the NF peak intensity versus field. (b) Zoom on the Er1 and Er2 Bragg peaks with an inset showing Er1 peak for $B = 0, 80$, and 100 kG.

the unit cell volume remains constant upon applied field. Small changes of the Er1 and Er2 peak intensities are also observed [Fig. 10(b)]. The variation of the $M(B)$ at 4.2 K (Sec. III B 1) was interpreted by a transition from a ferrimagnetic structure at low field towards a FM structure at high field. The transition between these two magnetic states can occur through several ways: (i) a relative rotation of the Fe and Er moments to form an angular structure that resultant align along the direction of the applied field [51] or (ii) a demagnetization of the Er moments as far as $B < B_{Trans}$ [52].

In order to determine which of these mechanisms is responsible for the observed transition, different simulations of the NPD patterns have been performed. As the Fe moments are stable in this temperature range and have a larger amplitude ($3.8 \mu_B \text{ f.u.}^{-1}$) than the Er moment contribution taking into account the proportion of each element ($1.8 \mu_B \text{ f.u.}^{-1}$), either a rotation or a demagnetization of the Er moments has been assumed. A rotation of the Er moments leads to a decrease of the NF peak intensity, a decrease of the Er1, and an increase of the Er2 peak intensities (the total magnetic peak intensity should remain constant if the Er moment keeps the same intensity). The demagnetization of the Er moment yields a decrease of all magnetic peak intensity. The observation of the change of the Er1 and Er2 peak intensity suggests first a small

rotation of the Er moments when the field increases from 0 to 30 kG and then a demagnetization for larger applied field [Fig. 10(b)]. Even at very low temperature, the Er1 and Er2 peak intensities are at the limit of the noise level. However, an optimistic sight of the Er1 peak variations versus B shows that the peak intensity decreases first when B is smaller than 80 kG and then increases up to 100 kG. Furthermore, as no extra peaks are induced by the B presence, an indirect confirmation of the Er demagnetization without change of spin orientation is then obtained although the signal to noise ratio is not large.

The demagnetization process should be followed by a further magnetization of Er moments at larger field, but the NPD measurements at 2 K were limited to 100 kG. This demagnetization process is favored by the strong anisotropy (Er and Fe moment lying in the plane perpendicular to the monoclinic b_{axis}) and the crystal field effect, which strongly reduces the Er moment amplitude. It is also worth noting that the measured $M_T(B)$ curves cross that of $\text{YFe}_2\text{D}_{4.2}$ at B_{Trans} , supporting the results that only Fe sublattice contributes to the magnetization at this crossing field. Such mechanism of the demagnetization of the rare earth moment has been observed on a $\text{Tm}_2\text{Co}_{17}$ single crystal [53]. A demagnetization

of both Er and Fe sublattices has been also observed at the compensation temperature (T_{Comp}) of $\text{ErFe}_2\text{D}_{3.5}$ by x-ray magnetic circular dichroism (XMCD) measurements at both Er- L_{III} edge and Fe K -edge [33]. In these experiments, a decrease of the XMCD signal intensity was observed when approaching T_{Comp} , followed by an inversion of the sign of the signals and an intensity increase versus temperature.

The intensities of the AFM and NF peaks, as well as the NF peak position (expressed in distance) of $\text{Y}_{0.7}\text{Er}_{0.3}\text{Fe}_2\text{D}_{4.2}$ compound at $T = 75$ K, are represented in Fig. 11. A decrease of the AFM peak intensity and an increase of the NF peak versus applied field are observed, confirming that an AFM-FM transition occurs versus applied field. This transition is also accompanied by a cell volume increase, which follows the variation of the magnetization at 75 K. Similar observations have been done at $T = 90$ and 100 K, confirming the first-order character of the field induced AFM-FM transition. The diminution of the NF peak intensity above 60 kG can be due to a contribution of an induced Er moment parallel to Fe, as will be discussed later (Sec. IV B).

At 90 kG, the NF peak intensity decreases linearly as T increases, with a discontinuity at 110 K (Supplemental Material, Fig. S3 [45]). This transition temperature is close to the value deduced from the $B_{\text{Trans}} = f(T)$ curve in Fig. 4 where a temperature of 102 K was found at $B = 90$ kG.

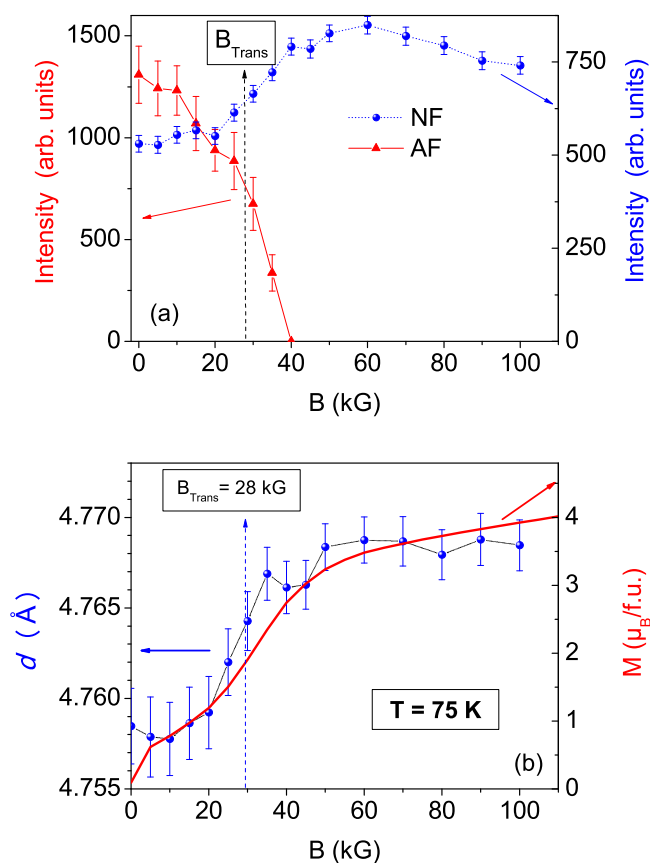


FIG. 11. Integrated intensities of the AF and NF peaks (a) and d interplanar distances of the NF peak (b) measured by NPD on $E6$ at $T = 75$ K. The $M_T(B)$ curve (line at the bottom figure) of $\text{Y}_{0.7}\text{Er}_{0.3}\text{Fe}_2\text{D}_{4.2}$ has been added for comparison. The dashed lines correspond to the transition field B_{Trans} [inflection point of the $M_T(B)$ curve].

IV. DISCUSSION

This experimental study on $\text{Y}_{0.7}\text{Er}_{0.3}\text{Fe}_2\text{D}_{4.2}$ has confirmed the existence of two different types of metamagnetic behavior depending on the temperature range. A schematic magnetic field-temperature phase diagram is presented in Fig. 12 to support the following discussion.

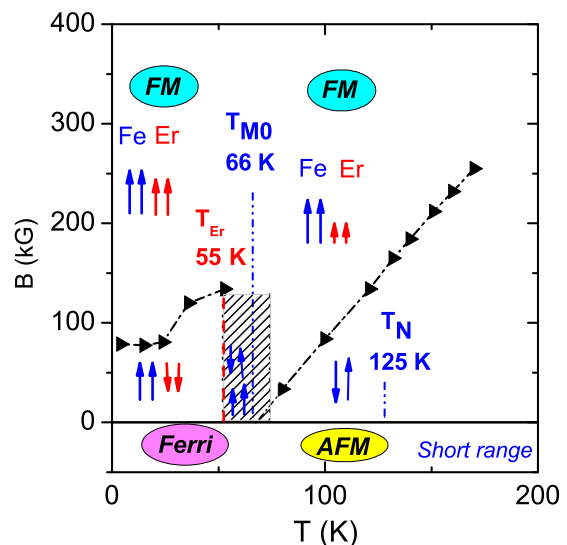


FIG. 12. Schematic phase diagram of $\text{Y}_{0.7}\text{Er}_{0.3}\text{Fe}_2\text{D}_{4.2}$ representing the relative orientations of the Fe and Er moments versus field and temperature. The Er and Fe moments are oriented perpendicular to the monoclinic b axis. The dashed zone indicates the coexistence of the FM and AFM structures.

A. Second-order type metamagnetic transition at low temperature

For $T < 55$ K, the magnetic ground state is ferrimagnetic: All the Fe atoms carry a magnetic moment [$m_{\text{Fe}} \approx 2.0(1)\mu_B$] and form a FM sublattice, which is antiparallel to the Er magnetic sublattice as long as B is absent. The Er and Fe moments are lying within the (a, c) basal plane. Above B_{Trans} , the arrangement between the Er and Fe sublattice is kept collinear under application of large magnetic field corresponding now to a FM ordering. In the infinite applied field, the low temperature Er magnetic moment is extrapolated to be very close to the free atom value. This metamagnetic behavior observed below 55 K can be therefore related to a ferrimagnetic-FM transition, which has been seldom observed in rare earth intermetallic compounds with Fe or Co transition metals and in these few cases at significantly higher transition fields. Note that for all these compounds, the magnetization curves were measured with pulsed magnetic fields, which do not allow us to maintain isothermal conditions, whereas in the present experiment the isothermal conditions were maintained. In $\text{Tm}_2\text{Co}_{17}$, a transition from a collinear ferrimagnetic ($M_s = 17m_{\text{Co}} - 2m_{\text{Tm}}$) to a FM state with parallel orientation of the Co and Tm sublattice ($M_s = 17m_{\text{Co}} + 2m_{\text{Tm}}$) along the c axis has been observed with a transition field of 390 kG at 4.2 K [53]. In isostructural $\text{Er}_2\text{Co}_{17}$, although a sharp magnetic transition is also observed at 400 kG, the parallel alignment of the Co and Er moment is not reached at 600 kG. In the $\text{Tm}_2\text{Fe}_{17}$ intermetallic compound, two field induced transitions are observed at 410 and 540 kG, along the c axis at 1.5 K, but the FM state is too far to be reached. In the corresponding hydride $\text{Tm}_2\text{Fe}_{17}\text{D}_{3.2}$, similar transitions are observed at 430 kG and 530 kG. The transition fields are therefore not significantly modified by D absorption in this system. Forced ferrimagnetic-FM transitions were observed at transition fields of 1.01–1.05 MG for DyFe_{14}B and 490 kG for TmFe_{14}B at 10 K [54] and at 600 kG for $\text{ErFe}_{11}\text{TiH}$ single crystal at 4.2 K [55].

It is therefore remarkable that in $\text{Y}_{0.7}\text{Er}_{0.3}\text{Fe}_2\text{D}_{4.2}$, a compound containing both Er and Fe, the ferrimagnetic-FM transition is observed with a transition field of only 78 kG for temperatures below 30 K. The conditions under which a forced FM state is reached has been related to the strength of the A-Fe intersublattice coupling [55]. Such a low transition field should therefore be explained by a larger weakening of the Er-Fe exchange interactions compared to the A_2Fe_{17} , $\text{A}_2\text{Fe}_{14}\text{B}$, and $\text{ErFe}_{11}\text{TiH}$ systems accompanied by a strong structural anisotropy, which constrains the orientation of the Er and Fe moments in the easy plane.

Hydrogen absorption is known to reduce the Ruderman-Kittel-Kasuya-Yosida (RKKY) indirect $4f$ - $3d$ exchange interactions as it increases the interatomic distances between the $4f$ and $3d$ magnetic atoms and modifies the electronic structure. For example, the molecular field B_m arising from the Fe sublattice on Er sublattice in ErFe_2H_y was found to decrease from 500 kG for $y = 0$ to 42 kG for $y = 3.9$ in Ref. [32]. A strong reduction of the total molecular field B_m was also observed by Deryagin *et al.* [31] on ErFe_2H_y single crystals. The latter observed also a rapid fall of the magnetocrystalline anisotropy constants upon H absorption. As in this paper, the

D content is larger than in previous studies, the weakening of the Er-Fe interactions should be stronger. In $\text{Y}_{0.7}\text{Er}_{0.3}\text{Fe}_2\text{D}_{4.2}$, the reduction of the Er-Fe interaction should therefore result from the increase of the Er-Fe interatomic distances (+8.3%) and the large number of D neighbors around each Er atom (7 to 7.8 D atoms) and Fe atoms (3.6 to 4.6 D atoms). The broad Er-Fe distance distribution due to the lowering of the crystal symmetry ($d_{\text{Er-Fe}}$ varies between 3.05 and 3.48 Å) can also be responsible for a weakening of these interactions.

The second important factor is the strong structural anisotropy induced by the lowering of the symmetry from cubic towards a monoclinic structure. The monoclinic b parameter remains constant, whereas the a and c parameters decrease down to $T_N = 150$ K, indicating an increase of the monoclinic distortion along the b axis upon cooling. The D insertion yields a doubling of the b cell parameter, and the Fe and Er moments are constrained to remain parallel to the basal plane.

This can explain the large crystal field effect, which reduces the Er moment to $6.4 \pm 0.3\mu_B$ compared to the Er free ion value ($9\mu_B$). A fanning scenario has been proposed in the case of ErFe_2 hydrides, with lower H content to explain the reduction of the Er moment [56–59]. But on the other hand, we found that orthorhombic ErFe_2D_5 forms a canted magnetic structure with $m_{\text{Er}} = 6.6\mu_B$ at 1.5 K [34]. As the mean Er moment in $\text{Y}_{0.7}\text{Er}_{0.3}\text{Fe}_2\text{D}_{4.2}$ is close to that refined in ErFe_2D_5 , in which Er moments order in a well-defined canted magnetic structure, its reduction should be rather attributed to the crystal field influence. In this crystal electric field effect scenario, when B increases in the 4.2–30 K range, the observed field-induced magnetic transition would result from a crossing of the energy levels of the Er atom in presence of applied field. However, the distinction between each individual magnetic Er moment and the average Er moment cannot be done. Between 30 and 55 K, the crossing of the lowest energy levels would become less and less pronounced, and the intensity of the metamagnetic transition would disappear progressively. It is remarked that according to the NPD refinement at zero field, m_{Er} decreases versus temperature approaching zero at 55 K. It may be added that the Er sublattice magnetization is too small to compete with the Fe one so that no compensation temperature is observed in $\text{Y}_{0.7}\text{Er}_{0.3}\text{Fe}_2\text{D}_{4.2}$ for the spontaneous state in the whole temperature range. Under very intense applied magnetic field, the crystal field effect disappears, and the mean Er moment becomes close to the free ion value.

Finally, the unusual features of this particular ferrimagnetic-FM field induced transition should be also considered: (i) the evolution from a reduced Er moment ($m_{\text{Er}} = 6.4 \pm 0.3\mu_B$) at low field and temperature toward a free ion value ($9\mu_B$) at high field, (ii) the mechanism of the transition through a demagnetization of Er moment such as in $\text{Tm}_2\text{Co}_{17}$, and (iii) the stability of the FM state up to at least 150 K. In previous work [42], it was also observed that the transition fields are equal to 78 kG below 30 K in both hydride and deuteride of $\text{Y}_{0.7}\text{Er}_{0.3}\text{Fe}_2$ and therefore not isotope sensitive.

B. First-order type AFM-FM metamagnetic transition above T_{M0}

Above 55 K, a first-order transition from a FM towards an AFM state occurs upon increasing temperature for the Fe

sublattice of $Y_{0.7}Er_{0.3}Fe_2D_{4.2}$, similar to that for $YFe_2D_{4.2}$. This transition is accompanied by a noticeable cell volume contraction, as often observed in first-order IEM transitions. In the spontaneous state, the AFM structure is described by doubling the lattice parameter b , the key result being that four Fe atoms (Fe7) out of 32 have no more ordered magnetic moments at the transition, as detailed in a previous study on the magnetic structure of $YFe_2(H,D)_{4.2}$ compounds. In presence of an external field, the field-induced transition is related to the AFM-FM transition.

It is remarked that the field induced transition continues to exist up to 175 K without a noticeable accident on the $B_{Trans}(T)$ variation, i.e., well above T_N ($T_N = 125$ K in zero applied field). This behavior is related to the short range distance interaction region, which exists just above T_N ; in this temperature region, an applied magnetic field is able to create a magnetic arrangement similar to that below T_N , including first the onset of the AFM ordering of the Fe magnetic moment and then the AFM-FM transition. The study of the shift of the magnetic peak positions versus field leads to an abrupt variation of the interplanar distances for the concerned NF peak. This variation under B application is negative when the transition takes place in the FM-AFM sense, as it was observed for $B = 0$ ($\Delta V/V = -0.58\%$). This conclusion is confirmed by the analysis of the magnetic peak shift when the transition is induced by an external field. On the contrary, for the low temperature field induced transition, no such peak shift was observed.

Compared to $YFe_2D_{4.2}$, we observe an additional increase of the magnetization due to the Er contribution, whose shape suggests a progressive transition toward a FM state with parallel Er and Fe sublattice [Fig. 3(c)]. This is also confirmed by the evolution of the saturation magnetization [Fig. 5(b)]. As above 55 K and zero field the Er sublattice is no more ordered, it means that in addition to the AFM-FM field induced transition of the Fe sublattice, a PM-FM transition of the Er sublattice should occur. As the spontaneous magnetization is weak and similar in both $YFe_2D_{4.2}$ and $Y_{0.7}Er_{0.3}Fe_2D_{4.2}$, the PM-FM transition occurs above B_{Trans} . An indication is the decrease of the NF Bragg peak intensity above B_{Trans} (Fig. 11), which can originate from the Er magnetic contribution. The molecular field B_m arising from the Fe sublattice in the FM state on Er probably favors the ordering of Er. This can also explain the larger dB_{Trans}/dT slope for the Er substituted compound (2.48 kG K $^{-1}$) compared to $YFe_2D_{4.2}$ (1.37 kG K $^{-1}$) (Fig. 4). On the contrary, in $Y_{0.7}Er_{0.3}Fe_2H_{4.2}$ the dB_{Trans}/dT slope was found slightly smaller (1.27 kG K $^{-1}$) [42]. As the Er magnetic behavior appears not very sensitive to the (H, D) isotope effect, the Er sublattice should order at about the same temperature in both hydride and deuteride (55 K), whereas T_{M0} is shifted to 107 K in the hydride due to magnetovolumic effect. The localized character of the $4f$ electronic shell is most probably at the origin of this low sensitivity of the Er magnetic behavior to the isotope nature.

Another important key result of our data analysis is the role of the cell volume of the deuteride: T_{M0} is shifted to lower value upon Er substitution (-28.6%), as expected from the cell volume reduction (-0.6%). Nevertheless, the Er for Y substitution cannot be considered as a simple chemical pressure effect on the magnetic properties when compared

to the influence of an external pressure. Indeed the variation of T_{M0} versus cell volume ($\Delta T_{M0}/\Delta V = -9$ K/ \AA^3) is smaller for the Er substitution compared to the value calculated for the measurements under pressure ($\Delta T_{M0}/\Delta V = -24$ K/ \AA^3) [40,41].

We may then conclude that the AFM-FM transition related to the Fe behavior is of first-order character in absence or in presence of applied field. On the other hand, the low temperature field induced transition is of the second-order type and is well described by the one atom model involving Er atoms.

More generally, this paper reveals that hydrogen or deuterium insertion can completely modify the magnetic properties of the AFe_2 type compounds ($R = Y$ or lanthanide) where the Fe has a stable moment and an elevated Curie temperature, and induces IEM behavior on the transition metal sublattice, as observed in ACo_2 and $(Hf,Ta)Fe_2$ compounds and weakens the Er-Fe interactions.

V. CONCLUSION

This paper has shown that $Y_{0.7}Er_{0.3}Fe_2D_{4.2}$ crystallizes in the same monoclinic nuclear structure ($P1c1$ space group) as $YFe_2D_{4.2}$ and that 30% Er substitution induces a 0.6% cell volume contraction.

The study of the magnetic properties shows two main influences of the Er substitution, both characterized by metamagnetic behavior of different physical origin. At low temperature, a forced ferrimagnetic-FM transition occurs at a moderate transition field (78 kG) in $Y_{0.7}Er_{0.3}Fe_2D_{4.2}$: The Er moments that are antiparallel to the Fe moments at low field become parallel to Fe and form a collinear FM structure. Such transition, which is rather seldom in rare-earth and Fe intermetallic is favored by the weak Er-Fe exchange interaction due to the large D content (increase of the interatomic distances, modification of the electronic structure) and the structure anisotropy. The Er moments that are reduced at low field due to crystal field effect become close to the free ion value at high field. The ferrimagnetic ground state is maintained up to 55 K. Above this temperature, the Er moments are no more ordered at zero field.

At $T_{M0} = 66$ K, a first-order transition from a FM towards an AFM state is observed for the Fe sublattice, such as that for $YFe_2D_{4.2}$ ($T_{M0} = 84$ K). The 18 K decrease of T_{M0} is only partially related to the cell volume reduction, as the $\Delta T_{M0}/\Delta V$ is smaller than observed when applying an external pressure. The Néel temperature is reduced by only 6 K by Er substitution. The field induced transition above T_{M0} corresponding to an AFM-FM transition of the Fe sublattice is accompanied by a cell volume increase, whereas an Er moment is induced above B_{Trans} due to the influence of B_m issued from Fe and the applied field. In addition to the large D induced reduction of the ordering temperature and the occurrence of IEM transition on the Fe sublattice, an evolution of the Fe magnetic character to a more delocalized one has been discussed

To conclude, it has been observed that the large deuterium insertion modifies the magnetic coupling between the itinerant $3d$ Fe moments, but not significantly their ground state magnitudes. On the contrary, in spite of its localized character, the mean $4f$ Er moment magnitude is sensitive to

the presence of deuterium nearest neighbors. Further studies will be performed to determine more systematically the influence of Er content on the metamagnetic transitions in $Y_{1-x}Er_xFe_2(H,D)_{4.2}$ compounds. The influence of the nature of the rare earth will be also investigated.

ACKNOWLEDGMENTS

The authors thank the Institute Laue Langevin (Grenoble, France), the Laboratoire Léon Brillouin (Saclay, France), and the Helmholtz Zentrum Berlin (Berlin, Germany) for the allocated neutron beam time to perform the NPD experiments. The authors are also grateful to the Laboratoire National des

Champs Magnétiques Intenses (LNCMI, Grenoble, France) for the allocated time given to perform high magnetic field measurements. This research project has been supported by the European Commission under the 6th Framework Programme through the Key Action: Strengthening the European Research Area, Research Infrastructures, Contract No. RII3-CT-2003-505925 (NMI3). We are thankful to Dr. Stuesser for his help on the experiment on the E6 spectrometer at HZB in Berlin. Finally, the authors warmly thank Dr. Mathieu Phejar for his participation and help during the neutron data acquisition in the Grenoble and Berlin neutron centers. V. Paul-Boncour dedicates this paper to the memory of her colleague Marcel Escorne, who participated in the first magnetic measurements regarding $YFe_2D_{4.2}$ and passed away in February 2017.

-
- [1] A. E. Clark, *Handbook on the Physics and Chemistry of Rare Earth*, edited by K. A. Gschneidner Jr. and L. Eyring (North-Holland Publishing Company, Amsterdam, 1979), Vol. 2, Chap. 15, pp. 231–258.
- [2] J. J. M. Franse and R. J. Radwanski, *Handbook of Magnetic Materials*, edited by K. H. J. Bushow (Elsevier Science Publishers, Amsterdam, 1993), Vol. 7, Chap. 5, pp. 307–501.
- [3] R. Ballou, C. Lacroix, and M. D. Nunez Regueiro, *J. Magn. Magn. Mater.* **104–107**, 753 (1992).
- [4] M. Shiga, *J. Magn. Magn. Mater.* **129**, 17 (1994).
- [5] C. Lacroix, B. Canals, M. D. Nunez-Regueiro, B. Coqblin, and J. Arispe, *Physica B* **230–232**, 529 (1997).
- [6] J. Zou, D. Paudyal, J. Liu, Y. Mudryk, V. K. Pecharsky, and K. A. Gschneidner, *J. Mater. Chem. C* **3**, 2422 (2015).
- [7] N. C. Koon, C. M. Williams, and B. N. Das, *J. Magn. Magn. Mater.* **100**, 173 (1991).
- [8] H. Uchida, Y. Matsumura, H. Uchida, and H. Kaneko, *J. Magn. Magn. Mater.* **239**, 540 (2002).
- [9] C. Morrison, D. Wang, G. J. Bowden, R. C. C. Ward, and P. A. J. d. Groot, *J. Appl. Phys.* **111**, 063917 (2012).
- [10] S. N. Gordeev, J. M. L. Beaujour, G. J. Bowden, B. D. Rainford, P. A. J. de Groot, R. C. C. Ward, M. R. Wells, and A. G. M. Jansen, *Phys. Rev. Lett.* **87**, 186808 (2001).
- [11] T. Goto, K. Fukamichi, T. Sakakibara, and H. Komatsu, *Solid State Commun.* **72**, 945 (1989).
- [12] T. Goto, T. Sakakibara, K. Murata, H. Komatsu, and K. Fukamichi, *J. Magn. Magn. Mater.* **90–91**, 700 (1990).
- [13] N. V. Baranov and A. I. Kozlov, *J. Alloys Compds* **190**, 83 (1992).
- [14] D. P. Kozlenko, E. Burzo, P. Vlais, S. E. Kichanov, A. V. Rutkauskas, and B. N. Savenko, *Sci. Rep.* **5**, 8620 (2015).
- [15] Y. Mudryk, D. Paudyal, A. K. Pathak, V. K. Pecharsky, and K. A. Gschneidner, *J. Mater. Chem. C* **4**, 4521 (2016).
- [16] J. Ćwik, T. Palewski, K. Nenkov, J. Warchulska, and J. Klamut, *J. Magn. Magn. Mat.* **324**, 677 (2012).
- [17] E. Gratz and A. S. Markosyan, *J. Phys.: Condens. Matter* **13**, R385 (2001).
- [18] T. Sakakibara, T. Goto, K. Yoshimura, M. Shiga, Y. Nakamura, and K. Fukamichi, *J. Magn. Magn. Mater.* **70**, 126 (1987).
- [19] K. Fujiwara, K. Ichinose, H. Nagai, and A. Tsujimura, *J. Magn. Magn. Mater.* **90/91**, 561 (1990).
- [20] R. Hauser, E. Bauer, E. Gratz, M. Rotter, H. Muller, G. Hilscher, H. Michor, and A. S. Markosyan, *Physica B* **239**, 83 (1997).
- [21] A. S. Markosyan, R. Hauser, M. Galli, E. Bauer, E. Gratz, G. Hilscher, K. Kamishima, and T. Goto, *J. Magn. Magn. Mater.* **185**, 235 (1998).
- [22] K. H. J. Buschow and R. P. Van Staple, *J. Appl. Phys.* **41**, 4066 (1970).
- [23] J. Ćwik, Y. Koshkid'ko, A. Mikhailova, N. Kolchugina, K. Nenkov, A. Hackamer, and M. Miller, *J. Appl. Phys.* **117**, 123912 (2015).
- [24] Y. Nishihara and Y. Yamaguchi, *J. Magn. Magn. Mater.* **31–34**, 77 (1983).
- [25] G. Kido, Y. Tadakuma, Y. Nakagawa, Y. Nishihara, and Y. Yamaguchi, *J. Magn. Magn. Mater.* **54–57**, 885 (1986).
- [26] L. V. B. Diop, Z. Arnold, and O. Isnard, *J. Magn. Magn. Mater.* **395**, 251 (2015).
- [27] L. V. B. Diop, D. Benea, S. Mankovsky, and O. Isnard, *J. Alloys Compds* **643**, 239 (2015).
- [28] Y. Zhu, K. Asamoto, Y. Nishimura, T. Kouen, S. Abe, K. Matsumoto, and T. Numazawa, *Cryogenics* **51**, 494 (2011).
- [29] G. Wiesinger and G. Hilscher, in *Handbook of Magnetic Materials*, Vol. 17, edited by K. H. J. Bushow (Elsevier North-Holland, Amsterdam, 2008), pp. 293–456.
- [30] I. Bigun, V. Smetana, Y. Mudryk, I. Hlova, M. Dzevenko, L. Havela, Y. Kalychak, V. Pecharsky, and A.-V. Mudring, *J. Mater. Chem. C* **5**, 2994 (2017).
- [31] A. V. Deryagin, N. V. Kudrevatykh, V. N. Moskalev, and N. V. Mushnikov, *Fiz. Metal. Metalloved.* **58**, 1148 (1984) [*Phys. Met. Metall.* **58**, 96 (1984)].
- [32] T. de Saxce, Y. Berthier, and D. Fruchart, *J. Less-Common Met.* **107**, 35 (1985).
- [33] V. Paul-Boncour, C. Giorgetti, G. Wiesinger, and A. Percheron-Guégan, *J. Alloys Compds* **356–357**, 195 (2003).
- [34] V. Paul-Boncour, S. M. Filipek, I. Marchuk, G. André, F. Bourée, G. Wiesinger, and A. Percheron-Guégan, *J. Phys.: Condens. Matter* **15**, 4349 (2003).
- [35] V. Paul-Boncour and S. F. Matar, *Phys. Rev. B* **70**, 184435 (2004).
- [36] V. Paul-Boncour, G. André, F. Bourée, M. Guillot, G. Wiesinger, and A. Percheron-Guégan, *Physica B* **350**, e27 (2004).
- [37] V. Paul-Boncour, M. Guillot, G. Wiesinger, and G. André, *Phys. Rev. B* **72**, 174430 (2005).
- [38] V. Paul-Boncour, M. Guillot, O. Isnard, B. Ouladdiaf, A. Hoser, T. Hansen, and N. Stuesser, *J. Solid State Chem.* **245**, 98 (2017).

- [39] J. Ropka, R. Cerny, V. Paul-Boncour, and T. Proffen, *J. Solid State Chem.* **182**, 1907 (2009).
- [40] O. Isnard, V. Paul-Boncour, Z. Arnold, C. V. Colin, T. Leblond, J. Kamarad, and H. Sugiura, *Phys. Rev. B* **84**, 094429 (2011).
- [41] O. Isnard, V. Paul-Boncour, and Z. Arnold, *Appl. Phys. Lett.* **102**, 122408 (2013).
- [42] M. Guillot, V. Paul-Boncour, and T. Leblond, *J. Appl. Phys.* **107**, 09E144 (2010).
- [43] T. Leblond, V. Paul-Boncour, and A. Percheron-Guégan, *J. Alloys Compds* **446–447**, 419 (2007).
- [44] J. Rodriguez-Carvajal, *Physica B* **192**, 55 (1993).
- [45] See Supplemental Material at <http://link.aps.org/supplemental/10.1103/PhysRevB.96.104440> for complementary figures and table related to the magnetic properties of $Y_{0.7}Er_{0.3}Fe_2D_{4.2}$.
- [46] V. Paul-Boncour and T. Mazet, *J. Appl. Phys.* **105**, 013914 (2009).
- [47] G. V. Brown, *J. Appl. Phys.* **47**, 3673 (1976).
- [48] P. Rhodes and E. P. Wohlfarth, *Proc. R. Soc. London, Ser. A* **273**, 247 (1963).
- [49] E. P. Wohlfarth, *J. Magn. Magn. Mater.* **7**, 113 (1978).
- [50] P. Westwood, J. S. Abell, and K. C. Pitman, *J. Appl. Phys.* **67**, 4998 (1990).
- [51] O. Isnard, Y. Skourski, L. V. B. Diop, Z. Arnold, A. V. Andreev, J. Wosnitza, A. Iwasa, A. Kondo, A. Matsuo, and K. Kindo, *J. Appl. Phys.* **11**, 093916 (2012).
- [52] O. Isnard, A. V. Andreev, M. D. Kuzmin, Y. Skourski, D. I. Gorbunov, J. Wosnitza, N. V. Kudrevatykh, A. Iwasa, A. Kondo, A. Matsuo, and K. Kindo, *Phys. Rev. B* **88**, 174406 (2013).
- [53] A. V. Andreev, M. D. Kuz'min, Y. Narumi, Y. Skourski, N. V. Kudrevatykh, K. Kindo, F. R. de Boer, and J. Wosnitza, *Phys. Rev. B* **81**, 134429 (2010).
- [54] H. Kato, D. W. Lim, M. Yamada, Y. Nakagawa, H. Aruga Katori, and T. Goto, *Physica B* **211**, 105 (1995).
- [55] N. V. Kostyuchenko, A. K. Zvezdin, E. A. Tereshina, Y. Skourski, M. Doerr, H. Drulis, I. A. Pelevin, and I. S. Tereshina, *Phys. Rev. B* **92**, 104423 (2015).
- [56] M. O. Bargouth and G. Will, *J. Phys. Colloques* **32**, C1-675 (1971).
- [57] D. Fruchart, Y. Berthier, T. de Saxce, and P. Vulliet, *J. Less-Common Met.* **130**, 89 (1987).
- [58] D. Fruchart, Y. Berthier, T. de Saxce, and P. Vulliet, *J. Solid State Chem.* **67**, 197 (1987).
- [59] P. J. Viccaro, G. K. Shenoy, B. D. Dunlap, D. G. Westlake, and J. F. Miller, *J. Phys. Colloques* **40**, C2-198 (1979).